A Beam Formulation with Shell Capabilities

Erasmo Carrera[1]
Department of Aeronautic and Space Engineering,
Politecnico di Torino, Torino, 10129, Italy

Marco Petrolo[2]
Department of Aeronautic and Space Engineering, Politecnico di Torino,
10129, Italy, and Institut Jean Le Rond d'Alembert,
UMR7190 CNRS, Paris06, 75252 Paris, France

Refined beam theories suitable for aerospace structures are presented in this paper. These theories have shell capabilities and permit the analysis of thin walled structures, such as wings and helicopter blades. The formulation is given in the framework of the Carrera Unified Formulation, CUF, which considers the order of the theory, N, as a free parameter of the analysis. N is the order of the 1D displacement expansion. The displacement components are, in fact, expanded in terms of the cross-section coordinates, (x, z), by using a set of 1-D generalized displacement variables. The refined kinematic models are based on Taylor-type polynomials. The finite element formulation is exploited in order to be able to face arbitrary cross-section geometries. FE's matrices are obtained in terms of a few fundamental nuclei which are formally independent of both N and the number of element nodes. A cubic (4 nodes) approximation along the beam axis, (y), is used. Structural analyses are conducted starting from classical beam theories, refined models are then introduced to evaluate non-classical effects. Different cross-section geometries, loading cases and boundary conditions are considered. It is mainly concluded that refined models are mandatory to properly detect shell-like mechanical behaviors. CUF hierarchical capabilities offer a powerful systematic procedure to implement higher-order beam theories with no constraints on N.

I. Introduction

The beam theory represents a reference technique to face the structural analysis of slender bodies such as airplane wings, helicopter blades and bridges. In all these cases, a beam model offers significant advantages with respect to more cumbersome two-dimensional, 2-D, and three-dimensional, 3-D, elements, because it permits the proper evaluation of the mechanical behavior of a structure via a 1-D analysis. Higher the order to which a beam theory is based on, higher its relevance. The refining process of a model is needed to detect non-classical effects such as shell-like responses.
Two main methods are recognizable in the developing of a beam theory: axiomatic and asymptotic. The former method establishes a kinematic model starting from the intuition of a scientist. The latter investigates the role played by the various variables of the model in terms of a perturbation parameter (usually a geometrical one such as the span-to-height ratio for beams). The 3-D problem is then reduced to a 1-D model by exploiting an asymptotic series of a characteristic parameter, and retaining those terms which exhibit the same order of magnitude when the perturbation parameter vanishes.

---

[1] Professor of Space Structures and Computational Aeroelasticity, Department of Aeronautic and Space Engineering, Politecnico di Torino, Corso Duca degli Abruzzi, 24, 10129 Torino, Italy, erasmo.carrera@polito.it.
[2] PhD Student, Department of Aeronautic and Space Engineering, Politecnico di Torino, Corso Duca degli Abruzzi, 24, 10129 Torino, Italy, marco.petrolo@polito.it., and Institut Jean Le Rond d'Alembert, UMR7190 CNRS, Paris06, Case 162, Tour 55-65, 4, Place Jussieu, 75252 Paris, France.

The Euler-Bernoulli and Timoshenko beam models are classical examples of axiomatic approaches. The former does not account for transverse shear effects on cross-section deformations. The latter provides a model that foresees a constant shear deformation distribution on the cross-section. Both of them yield better results for slender than for short beams. Important contributions on the development of refined theories by using an axiomatic approach have been furnished by Kapania [1, 2] and Eisenberger [3]. Examples of asymptotic based refined theories can be found in works by Volovoi et alii [4] and Yu et alii [5, 6].
Higher-order beam theories are herein developed in the framework of the Carrera Unified Formulation, CUF, which was initially developed for plates and shells [7, 8], and it has recently been extended to beams [9–13]. CUF offers a systematic procedure to obtain refined structural models by considering the order of the theory, N, as a free parameter of the formulation. Cubic beam elements (4 nodes) as well as different higher-order models for the cross-section displacement field are used. The Euler-Bernoulli and Timoshenko beam models are obtained as particular cases of the linear formulation. The results are compared with benchmarks retrieved from the classical models and with shell and solid models.

II. Preliminaries

The adopted coordinate frame is presented in Fig. 1. The beam boundaries over y are $0 \leq y \leq L$. The displacements vector is:

$$\mathbf{u}(x,y,z) = \left\{ \begin{array}{ccc} u_x & u_y & u_z \end{array} \right\}^T \tag{1}$$

Superscript "T" represents the transposition operator. The stress, $\boldsymbol{\sigma}$, and the strain, $\boldsymbol{\epsilon}$, are grouped as follows:

$$\begin{array}{l} \boldsymbol{\sigma}_p = \left\{ \begin{array}{ccc} \sigma_{zz} & \sigma_{xx} & \sigma_{zx} \end{array} \right\}^T, \quad \boldsymbol{\epsilon}_p = \left\{ \begin{array}{ccc} \epsilon_{zz} & \epsilon_{xx} & \epsilon_{zx} \end{array} \right\}^T \\ \boldsymbol{\sigma}_n = \left\{ \begin{array}{ccc} \sigma_{zy} & \sigma_{xy} & \sigma_{yy} \end{array} \right\}^T, \quad \boldsymbol{\epsilon}_n = \left\{ \begin{array}{ccc} \epsilon_{zy} & \epsilon_{xy} & \epsilon_{yy} \end{array} \right\}^T \end{array} \tag{2}$$

Subscript "n" stands for terms laying on the cross-section, while "p" stands for terms laying on planes orthogonal to Ω. Linear strain-displacement relations are used:

$$\begin{array}{l} \boldsymbol{\epsilon}_p = \boldsymbol{D}_p \mathbf{u} \\ \boldsymbol{\epsilon}_n = \boldsymbol{D}_n \mathbf{u} = (\boldsymbol{D}_{n\Omega} + \boldsymbol{D}_{nz}) \mathbf{u} \end{array} \tag{3}$$

with:

$$\boldsymbol{D}_p = \begin{bmatrix} 0 & 0 & \frac{\partial}{\partial z} \\ \frac{\partial}{\partial x} & 0 & 0 \\ \frac{\partial}{\partial z} & 0 & \frac{\partial}{\partial x} \end{bmatrix}, \quad \boldsymbol{D}_{n\Omega} = \begin{bmatrix} 0 & 0 & 0 \\ 0 & \frac{\partial}{\partial x} & 0 \\ 0 & \frac{\partial}{\partial z} & 0 \end{bmatrix}, \quad \boldsymbol{D}_{ny} = \begin{bmatrix} 0 & \frac{\partial}{\partial y} & 0 \\ \frac{\partial}{\partial y} & 0 & 0 \\ 0 & 0 & \frac{\partial}{\partial y} \end{bmatrix} \tag{4}$$

The Hooke law is exploited:

$$\boldsymbol{\sigma} = \boldsymbol{C} \boldsymbol{\epsilon} \tag{5}$$

According to Eq.s 2, the previous equation becomes:

$$\begin{array}{l} \boldsymbol{\sigma}_p = \tilde{\boldsymbol{C}}_{pp} \boldsymbol{\epsilon}_p + \tilde{\boldsymbol{C}}_{pn} \boldsymbol{\epsilon}_n \\ \boldsymbol{\sigma}_n = \tilde{\boldsymbol{C}}_{np} \boldsymbol{\epsilon}_p + \tilde{\boldsymbol{C}}_{nn} \boldsymbol{\epsilon}_n \end{array} \tag{6}$$

In the case of isotropic material the matrices $\tilde{\boldsymbol{C}}_{pp}$, $\tilde{\boldsymbol{C}}_{nn}$, $\tilde{\boldsymbol{C}}_{pn}$ and $\tilde{\boldsymbol{C}}_{np}$ are:

$$\tilde{\boldsymbol{C}}_{pp} = \begin{bmatrix} \tilde{C}_{11} & \tilde{C}_{12} & 0 \\ \tilde{C}_{12} & \tilde{C}_{22} & 0 \\ 0 & 0 & \tilde{C}_{66} \end{bmatrix}, \quad \tilde{\boldsymbol{C}}_{nn} = \begin{bmatrix} \tilde{C}_{55} & 0 & 0 \\ 0 & \tilde{C}_{44} & 0 \\ 0 & 0 & \tilde{C}_{33} \end{bmatrix}, \quad \tilde{\boldsymbol{C}}_{pn} = \tilde{\boldsymbol{C}}_{np}^T = \begin{bmatrix} 0 & 0 & \tilde{C}_{13} \\ 0 & 0 & \tilde{C}_{23} \\ 0 & 0 & 0 \end{bmatrix} \tag{7}$$

For the sake of brevity, the dependence of the coefficients $[\tilde{C}]_{ij}$ versus Young's moduli and Poisson's ratio is not reported here. It can be found in Tsai [14] or Reddy [15].

III. Unified Formulation.

In the framework of the Carrera Unified Formulation (CUF), the displacement field is assumed as an expansion in terms of generic functions, F_τ:

$$\mathbf{u} = F_\tau \mathbf{u}_\tau, \qquad \tau = 1, 2, ..., M \tag{8}$$

where F_τ are functions of the coordinates x and z on the cross-section. $\mathbf{u}_\tau$ is the displacement vector and M stands for the number of terms of the expansion. According to the Einstein notation, the repeated subscript τ indicates summation. Eq. (8) consists of a Maclaurin expansion that used as base the 2D polynomials $x^i\ y^j$, where i and j are positive integers. The maximum expansion order, N, is supposed to be 4. Table 1 presents M and F_τ as functions of N. For example, the second-order displacement field is:

$$\begin{array}{l} u_x = u_{x_1} + x\ u_{x_2} + z\ u_{x_3} + x^2\ u_{x_4} + xz\ u_{x_5} + z^2\ u_{x_6} \\ u_z = u_{y_1} + x\ u_{y_2} + z\ u_{z_3} + x^2\ u_{z_4} + xz\ u_{z_5} + z^2\ u_{z_6} \\ u_z = u_{z_1} + x\ u_{z_2} + z\ u_{z_3} + x^2\ u_{z_4} + xz\ u_{z_5} + z^2\ u_{z_6} \end{array} \tag{9}$$

The Timoshenko beam model (TBM) can be obtained by acting on the F_τ expansion. Two conditions have to be imposed. 1) a first-order approximation kinematic field:

$$\begin{array}{l} u_x = u_{x_1} + x\ u_{x_2} + z\ u_{x_3} \\ u_y = u_{y_1} + x\ u_{y_2} + z\ u_{y_3} \\ u_z = u_{z_1} + x\ u_{z_2} + z\ u_{z_3} \end{array} \tag{10}$$

2) the displacement components u_x and u_z have to be constant above the cross-section:

$$u_{x_2} = u_{z_2} = u_{x_3} = u_{z_3} = 0 \tag{11}$$

The Euler-Bernoulli beam (EBBM) can be obtained through the penalization of ϵ_{xy} and ϵ_{zy}. This condition can be imposed by using a penalty value χ in the following constitutive equations:

$$\begin{array}{l} \sigma_{xy} = \chi \tilde{C}_{55} \epsilon_{xy} + \chi \tilde{C}_{45} \epsilon_{zy} \\ \sigma_{zy} = \chi \tilde{C}_{45} \epsilon_{xy} + \chi \tilde{C}_{44} \epsilon_{zy} \end{array} \tag{12}$$

The classical theories and the first-order models require the assumption of opportunely reduced material stiffness coefficients to correct Poisson's locking (see Carrera and Brischetto [16, 17]). Unless differently specified, for classical and first-order models Poisson's locking is corrected according to Carrera and Giunta [9].
Introducing the shape functions, N_i, and the nodal displacement vector, $\mathbf{q}_{\tau i}$:

$$\mathbf{q} = \left\{ \begin{array}{ccc} q_{u_{x_{\tau i}}} & q_{u_{y_{\tau i}}} & q_{u_{z_{\tau i}}} \end{array} \right\}^T \tag{13}$$

The displacement vector becomes:

$$\mathbf{u}_\tau = N_i F_\tau \mathbf{q}_{\tau i} \tag{14}$$

For the sake of brevity, the shape functions are not reported here. They can be found in many books, for instance in [18]. Elements with 4 nodes (B4) are formulated, that is, a cubic approximation along the y axis is adopted. It has to be highlighted that, while the order of the beam model is related to the expansion on the cross-section, the number of nodes per each element is related to the approximation along the longitudinal axis. These two parameters are totally free and not related to each others. An N-order beam model is therefore a theory which exploits an N-order polynomial to describe the kinematics of the cross-section. The stiffness matrix of the elements and the external loadings, which are consistent with the model, are obtained via the Principle of Virtual

Displacements:

$$\delta L_{int} = \int_V (\delta \boldsymbol{\epsilon}_p^T \boldsymbol{\sigma}_p + \delta \boldsymbol{\epsilon}_n^T \boldsymbol{\sigma}_n) dV = \delta L_{ext} \tag{15}$$

Where L_{int} stands for the strain energy, and L_{ext} is the work of the external loadings. δ stands for the virtual variation. The virtual variation of the strain energy is rewritten using Eq.s (3), (6) and (14), in a compact format it becomes:

$$\delta L_{int} = \delta \mathbf{q}_{\tau i}^T \mathbf{K}^{ij\tau s} \mathbf{q}_{sj} \tag{16}$$

Where $\mathbf{K}^{ij\tau s}$ is the stiffness matrix in the form of the fundamental nucleus. Its components are:

$$\begin{aligned}
K_{xx}^{ij\tau s} = {} & \tilde{C}_{22} \int_\Omega F_{\tau,x} F_{s,x} d\Omega \int_l N_i N_j dy + \tilde{C}_{66} \int_\Omega F_{\tau,z} F_{s,z} d\Omega \int_l N_i N_j dy + \\
& \tilde{C}_{44} \int_\Omega F_\tau F_s d\Omega \int_l N_{i,y} N_{j,y} dy \\
K_{xy}^{ij\tau s} = {} & \tilde{C}_{23} \int_\Omega F_{\tau,x} F_s d\Omega \int_l N_i N_{j,y} dy + \tilde{C}_{44} \int_\Omega F_\tau F_{s,x} d\Omega \int_l N_{i,y} N_j dy \\
K_{xz}^{ij\tau s} = {} & \tilde{C}_{12} \int_\Omega F_{\tau,x} F_{s,z} d\Omega \int_l N_i N_j dy + \tilde{C}_{66} \int_\Omega F_{\tau,z} F_{s,x} d\Omega \int_l N_i N_j dy \\
K_{yx}^{ij\tau s} = {} & \tilde{C}_{44} \int_\Omega F_{\tau,x} F_s d\Omega \int_l N_i N_{j,y} dy + \tilde{C}_{23} \int_\Omega F_\tau F_{s,x} d\Omega \int_l N_{i,y} N_j dy \\
K_{yy}^{ij\tau s} = {} & \tilde{C}_{55} \int_\Omega F_{\tau,z} F_{s,z} d\Omega \int_l N_i N_j dy + \tilde{C}_{44} \int_\Omega F_{\tau,x} F_{s,x} d\Omega \int_l N_i N_j dy + \\
& \tilde{C}_{33} \int_\Omega F_\tau F_s d\Omega \int_l N_{i,y} N_{j,y} dy \\
K_{yz}^{ij\tau s} = {} & \tilde{C}_{55} \int_\Omega F_{\tau,z} F_s d\Omega \int_l N_i N_{j,y} dy + \tilde{C}_{13} \int_\Omega F_\tau F_{s,z} d\Omega \int_l N_{i,y} N_j dy \\
K_{zx}^{ij\tau s} = {} & \tilde{C}_{12} \int_\Omega F_{\tau,z} F_{s,x} d\Omega \int_l N_i N_j dy + \tilde{C}_{66} \int_\Omega F_{\tau,x} F_{s,z} d\Omega \int_l N_i N_j dy \\
K_{zy}^{ij\tau s} = {} & \tilde{C}_{13} \int_\Omega F_{\tau,z} F_s d\Omega \int_l N_i N_{j,y} dy + \tilde{C}_{55} \int_\Omega F_\tau F_{s,z} d\Omega \int_l N_{i,y} N_j dy \\
K_{zz}^{ij\tau s} = {} & \tilde{C}_{11} \int_\Omega F_{\tau,z} F_{s,z} d\Omega \int_l N_i N_j dy + \tilde{C}_{66} \int_\Omega F_{\tau,x} F_{s,x} d\Omega \int_l N_i N_j dy + \\
& \tilde{C}_{55} \int_\Omega F_\tau F_s d\Omega \int_l N_{i,y} N_{j,y} dy
\end{aligned} \tag{17}$$

The virtual variation of the work of the inertial loadings is:

$$\delta L_{ine} = \int_V \rho \ddot{\mathbf{u}} \delta \mathbf{u}^T dV \tag{18}$$

where ρ stands for the density of the material, and $\ddot{\boldsymbol{u}}$ is the acceleration vector. Eq. 18 is rewritten using Eq.s 3, and 14:

$$\delta L_{ine} = \int_l \delta \mathbf{q}_{\tau i}^T N_i \left[\int_\Omega \rho (F_\tau \mathbf{I})(F_s \mathbf{I}) d\Omega \right] N_j \ddot{\mathbf{q}}_{sj} dy \tag{19}$$

where $\ddot{\boldsymbol{q}}$ is the nodal acceleration vector. The last equation can be rewritten in the following compact manner:

$$\delta L_{ine} = \delta \mathbf{q}_{\tau i}^T \mathbf{M}^{ij\tau s} \ddot{\mathbf{q}}_{sj} \tag{20}$$

where $\mathbf{M}^{ij\tau s}$ is the mass matrix in the form of the fundamental nucleus. Its components are:

$$\begin{gathered} M_{xx}^{ij\tau s} = M_{yy}^{ij\tau s} = M_{zz}^{ij\tau s} = \rho \int_\Omega F_\tau F_s d\Omega \int_l N_i N_j dy \\ M_{xy}^{ij\tau s} = M_{xz}^{ij\tau s} = M_{yx}^{ij\tau s} = M_{yz}^{ij\tau s} = M_{zx}^{ij\tau s} = M_{zy}^{ij\tau s} = 0 \end{gathered} \tag{21}$$

It should be noted that no assumptions on the approximation order have been done. It is therefore possible to obtain refined beam models without changing the formal expression of the nucleus components. This is the key-point of CUF which permits, with only nine FORTRAN statements, to implement any-order beam theories. The shear locking is corrected through the selective integration (see [18]). The undamped dynamic problem can be written as it follows:

$$\boldsymbol{M}\ddot{\boldsymbol{a}} + \boldsymbol{K}\boldsymbol{a} = \boldsymbol{p} \tag{22}$$

where $\boldsymbol{a}$ is the vector of the nodal unknowns and $\boldsymbol{p}$ is the loadings vector. Introducing harmonic solutions, it is possible to compute the natural frequencies, ω_i, for the homogenous case, by solving an eigenvalues problem:

$$(-\omega_i^2 \mathbf{M} + \mathbf{K})\boldsymbol{a}_i = 0 \tag{23}$$

where $\boldsymbol{a}_i$ is the *i-th* eigenvector.

IV. Numerical results

Different static and dynamic assessments are considered hereafter. Previous works have dealt with the structural investigation of airfoil-shaped beams and unconventional wing configurations. The deformed free-tip cross-section of a cantilevered three-cell wing which undergoes a torsional loading is shown in Fig. 2 [11]. This result has been obtained via a fourth-order model, the out-of-plane warping is clearly detected. Fig. 3 [19] shows a natural mode of a joined-wing which has been obtained with the CUF beam and an MSC Nastran shell model. The comparison of the natural frequencies highlights an almost perfect agreement.

A simply supported beam with a thin-walled annular cross-section is considered as a first assessment of the present work. The geometric characteristics of the model are shown in Fig. 4. The outer diameter, d, is equal to 2 [m]. The thickness is supposed to be as high as 0.02 [m]. The length-to-diameter ratio, L/d, is equal to 10. An isotropic material is used. The Young modulus, E, is equal to 75 [GPa]. The Poisson ratio, ν, is equal to 0.33. A vertical force, P_{u_z}, is applied in [0, $L/2$, 1] and it is equal to 12.5 [MN]. The mechanical behavior of the structure is investigated through the vertical displacement of two points. The first one, T, coincides with the loading point, the latter, B, is placed at [0, $L/2$, -1]. A reference value is obtained via the following formula:

$$u_{z_b} = \frac{P_{u_z} L^3}{48 E I} \tag{24}$$

Where I is the cross-section moment of inertia. u_{z_B} and u_{z_T} are reported for increasing order beam models in Table 2. EBBM and TBM predict the same vertical displacement for both points. In particular, the Timoshenko beam shows a smaller rigidity. Linear and parabolic models furnish

slightly different results. It has to be highlighted that the second-order model gives a smaller displacement value than the first-order one because the Poisson locking correction is activated only for linear expansions. Remarkable differences are present in the solutions obtained through cubic and fourth-order models. u_{z_B} is considerably smaller than in case of lower-order expansions. This effect is related to the increase of u_{z_T} which is the vertical displacement of the point where the load is applied. u_{z_T} exploits a larger quote of the external work making the local effects more relevant than the global ones. This mechanical response is due to the presence of the concentrated load and is not detected at all by lower than cubic theories. This aspect is further clarified by Fig. 5. Linear and fourth-order models are compared by considering the deformed cross-sections at $y = L/2$. The deformability of the cross-section is not detectable by the linear model.
A clamped-clamped beam with a thin-walled annular cross-section is considered as the second assessment of the proposed model. The geometrical and material features are the same of the first case. The static analysis is conducted by applying a vertical force, P_{u_z}, equal to 5.0 [MN] at [0, $L/2$, 1]. Table 3 presents the vertical displacements of the loading point for different beam models. The last row is related to a shell model solution which has been made in MSC Nastran. The second column shows the total number of degrees of freedom of each model, that is, the computational cost. A good convergent behavior is observed with a considerable smaller computational effort than that required by the shell model. Fig. 6 shows the deformed configurations of the beam for different theories. EBBM is not able to detect the local effects of the concentrated load. Higher the order, more detailed the result becomes. A further investigation is furnished in Fig. 7 where the deformed loading point cross-sections are reported for different beam theories and compared with that obtained by MSC Nastran. It can be observed that models higher then the fourth are able to detect the displacement field of all the cross-section points but the loading one. It occurs models higher than the tenth-order to obtain a detailed description of the loading point displacement field. The free vibration analysis of the clamped-clamped model has been made as the last assessment of this work. Table 4 reports the first two bending frequencies for different beam models. Shell and solid models have been used for comparison purposes. The position within the eigenvalue vector of each frequency is shown in the superscripts. Each frequency appears twice because of the symmetry of the cross-section. The first bending frequency is properly detected by the third-order model although a fourth-order model is needed to predict the exact position of the frequency in the eigenvalue vector. A fifth-order model is needed to detect the second bending frequency whereas a sixth-order theory is able to exactly locate the position of the frequency in the eigenvalue vector. Fig.s 8, 9 shows two natural circumferential modes of the beam which are characterized by the presence of two and three lobes along the cross-section. Table 5 presents the natural frequencies of the first two-lobe mode for different theories. At least a third-order model is needed to detect this mode. The proper evaluation of the value of the natural frequency is furnished by the seventh-order model. It is significant to observe that the shell and the seventh-order beam model are able to compute a lower frequency than the solid one, that is, these two models are able to predict a lower stiffness of the model than that of the 3D elements. The first three-lobe mode frequencies are reported in Table 6. A fourth-order model is needed to detect this mode. The eighth-order model is able to furnish the same natural frequency of the shell model. The differences with the 3D elements are more relevant than in the two-lobe case.

V. Conclusion

The static and free vibration analyses of thin-walled structures based on higher-order beam theories have been presented in this paper. The Carrera Unified Formulation, CUF, has been used for the systemic implementation of refined models. According to CUF, the element stiffness and mass matrices are obtained in compact forms, named fundamental nuclei, that do not depend on the theory approximation order, that is, the order of the model is assumed as a free parameter of the modelling. Elements based on classical theories have been derived as particular cases. The numerical analyses have been conducted for the investigation of the static and dynamic behaviors in terms of deformed configurations, natural frequencies, and vibration modes. Comparisons with shell and solid models of commercial FE codes have been made. The following main conclusions can be drawn.

1. The builded beam formulation permits to deal in an unified manner with arbitrary cross-

section geometries and thin-walled structures.

2. The use of higher-order theories has permitted the overcome classical beam model limitations.

3. The comparison with shell and solid models has shown the shell capabilities of the refined beam theories in detecting the localized effects of concentrated loads and shell-like natural modes.

4. The computational effort requested by the present beam model is strongly smaller than those needed by shell and solid elements.

The use of the proposed beam models appears suitable for aeroelastic applications that include airfoil in-plane and out-of-plane deformations and for extensions to wings made of advanced composite materials. These topics could be subject of future works.

Acknowledgments

The financial support from the Regione Piemonte project MICROCOST is gratefully acknowledged.

References

[1] Kapania, K. and Raciti, S., "Recent Advances in Analysis of Laminated Beams and Plates, Part I: Shear Effects and Buckling," *AIAA JOURNAL*, Vol. 27, No. 7, 1989, pp. 923–935.

[2] Kapania, K. and Raciti, S., "Recent Advances in Analysis of Laminated Beams and Plates, Part II: Vibrations and Wave propagation," *AIAA JOURNAL*, Vol. 27, No. 7, 1989, pp. 935–946.

[3] Eisenberger, M., "An exact high order beam element," *Computers and Structures*, Vol. 81, 2003, pp. 147–152.

[4] Volovoi, V. V., Hodges, D. H., Berdichevsky, V. L., and Sutyrin, V. G., "Asymptotic theory for static behavior of elastic anisotropic I-beams," *International Journal of Solid Structures*, Vol. 36, 1999, pp. 1017–1043.

[5] Yu, W. and Hodges, D. H., "Elasticity Solutions Versus Asymptotic Sectional Analysis of Homogeneous, Isotropic, Prismatic Beams," *Journal of Applied Mechanics*, Vol. 71, 2004, pp. 15–23.

[6] Yu, W., Volovoi, V. V., Hodges, D. H., and Hong, X., "Validation of the variational asymptotic beam sectional analysis (VABS)," *AIAA Journal*, Vol. 40, 2002, pp. 2105–2113.

[7] Carrera, E., "Theories and finite elements for multilayered plates and shells," *Archives of Computational Methods in Engineering*, Vol. 9, No. 2, 2002, pp. 87–140.

[8] Carrera, E., "Theories and finite elements for multilayered plates and shells: a unified compact formulation with numerical assessment and benchmarking," *Archives of Computational Methods in Engineering*, Vol. 10, No. 3, 2003, pp. 216–296.

[9] Carrera, E. and Giunta, G., "Refined beam theories based on Carrera's Unified Formulation," *International Journal of Applied Mechanics*, In Press.

[10] Giunta, G., Carrera, E., and Belouettar, S., "A Refined Beam Theory with only Displacement Variables and Deformable Cross-Section," *50th AIAA/ASME/ASCE/AHS/ASC Structures, Structural Dynamics, and Materials Conference, Palm Springs, California 4 - 7 May 2009*, 2009.

[11] Carrera, E., Giunta, G., Nali, P., and Petrolo, M., "Refined beam elements with arbitrary cross-section geometries," *Computers and Structures*, Vol. 88, No. 5–6, 2010, pp. 283–293, DOI: 10.1016/j.compstruc.2009.11.002.

[12] Carrera, E., Petrolo, M., and Nali, P., "Unified formulation applied to free vibrations finite element analysis of beams with arbitrary section," *Shock and Vibrations*, Vol. 17, 2010, pp. 1–18, DOI: 10.3233/SAV-2010-0528.

[13] Carrera, E. and Petrolo, M., "On the Effectiveness of Higher-Order Terms in Refined Beam Theories," *Journal of Applied Mechanics*, In Press.

[14] Tsai, S. W., *Composites Design*, Dayton, Think Composites, 4th ed., 1988.

[15] Reddy, J. N., *Mechanics of laminated composite plates and shells. Theory and Analysis*, CRC Press, 2nd ed., 2004.

[16] Carrera, E. and Brischetto, S., "Analysis of thickness locking in classical, refined and mixed multilayered plate theories," *Composite Structures*, Vol. 82, No. 4, 2008, pp. 549–562.

[17] Carrera, E. and Brischetto, S., "Analysis of thickness locking in classical, refined and mixed theories for layered shells," *Composite Structures*, Vol. 85, No. 1, 2008, pp. 83–90.

[18] Bathe, K., *Finite element procedure*, Prentice hall, 1996.

[19] Carrera, E., Petrolo, M., and Varello, A., "Advanced Beam Formulations for Free Vibration Analysis of Conventional and Joined Wings," Submitted.

Tables

Table 1 Mac Laurin's polynomials.

N	M	F_τ
0	1	$F_1 = 1$
1	3	$F_2 = x \quad F_3 = z$
2	6	$F_4 = x^2 \quad F_5 = xz \quad F_6 = z^2$
3	10	$F_7 = x^3 \quad F_8 = x^2 z \quad F_9 = xz^2 \quad F_{10} = z^3$
...	...	...
N	$\frac{(N+1)(N+2)}{2}$	$F_{\frac{(N^2+N+2)}{2}} = x^N \quad F_{\frac{(N^2+N+4)}{2}} = x^{N-1}z \quad \dots \quad F_{\frac{N(N+3)}{2}} = xz^{N-1} \quad F_{\frac{(N+1)(N+2)}{2}} = z^N$

Table 2 Vertical displacements of different cross-section points computed via increasing order beam elements, simply-supported beam.

	u_{z_T} [m]	u_{z_B} [m]
Ref. Sol. Eq. 24	−0.456	−0.456
EBBM	−0.456	−0.456
TBM	−0.474	−0.474
N = 1	−0.475	−0.472
N = 2	−0.474	−0.467
N = 3	−0.644	−0.339
N = 4	−0.928	−0.159

Table 3 u_z displacements at the loading point for different beam theories and comparison with a shell model, clamped-clamped beam.

Theory	DOF's	u_z [m]
EBBM	155	−0.046
TBM	155	−0.053
N = 1	279	−0.053
N = 2	558	−0.052
N = 3	930	−0.114
N = 4	1395	−0.229
N = 5	1953	−0.335
N = 6	2604	−0.386
N = 7	3348	−0.486
N = 8	4185	−0.535
N = 9	5115	−0.564
N = 10	6138	−0.584
N = 11	7254	−0.597
Shell	49500	−0.670

Table 4 First two bending mode frequencies of the hollow cylinder and their position in the eigenvalue vector for different beam theories and comparison with shell and solid models, clamped-clamped beam.

Theory	DOF's	f_1 [Hz]	f_2 [Hz]
EBBM	155	$32.598^{1,2^*}$	$88.072^{3,4}$
TBM	155	$30.304^{1,2}$	$76.447^{3,4}$
N = 1	279	$30.304^{1,2}$	$76.447^{3,4}$
N = 2	558	$30.730^{1,2}$	$77.338^{3,4}$
N = 3	930	$28.754^{1,2}$	$69.448^{5,6}$
N = 4	1395	$28.747^{3,4}$	$69.402^{9,10}$
N = 5	1953	$28.745^{3,4}$	$69.397^{13,14}$
N = 6	2604	$28.745^{3,4}$	$69.397^{17,18}$
Shell	49500	$28.489^{3,4}$	$68.940^{17,18}$
Solid	174000	$28.369^{3,4}$	$68.687^{17,18}$

(∗): positions of the frequencies in the eigenvalue vector.

Table 5 First two-lobe mode frequencies of the hollow cylinder and their position in the eigenvalue vector for different beam theories and comparison with shell and solid models, clamped-clamped beam.

Theory	DOF's	f [Hz]
EBBM	155	–
TBM	155	–
N = 1	279	–
N = 2	558	–
N = 3	930	$38.755^{3,4^*}$
N = 4	1395	$25.156^{1,2}$
N = 5	1953	$20.501^{1,2}$
N = 6	2604	$20.450^{1,2}$
N = 7	3348	$17.363^{1,2}$
Shell	49500	$17.406^{1,2}$
Solid	174000	$18.932^{1,2}$

(∗): positions of the frequencies in the eigenvalue vector.

Table 6 First three-lobe mode frequencies of the hollow cylinder and their position in the eigenvalue vector for different beam theories and comparison with shell and solid models, clamped-clamped beam.

Theory	DOF's	f [Hz]
EBBM	155	–
TBM	155	–
N = 1	279	–
N = 2	558	–
N = 3	930	–
N = 4	1395	$75.690^{11,12}$
N = 5	1953	$65.186^{9,10}$
N = 6	2604	$52.386^{9,10}$
N = 7	3348	$50.372^{7,8}$
N = 8	4185	$40.102^{7,8}$
Shell	49500	$40.427^{7,8}$
Solid	174000	$46.444^{7,8}$

(∗): positions of the frequencies in the eigenvalue vector.

Figures

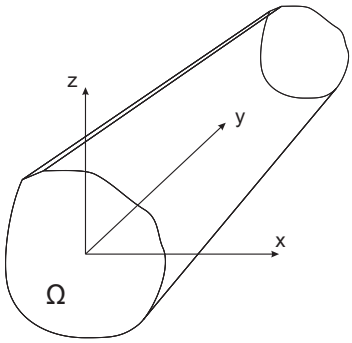

Fig. 1 Coordinate frame of the beam model.

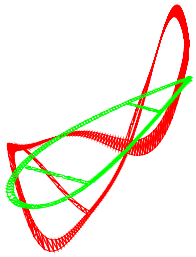

Fig. 2 Torsion analysis of a wing model via a fourth-order beam model.

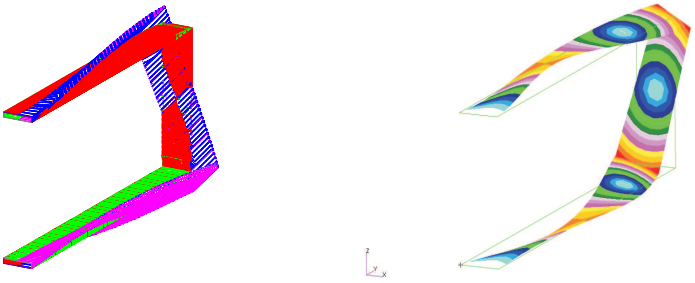

Fig. 3 Natural mode of a joined-wing via CUF, $f = 47.512$ [Hz], and MSC Nastran Shell, $f = 47.118$ [Hz].

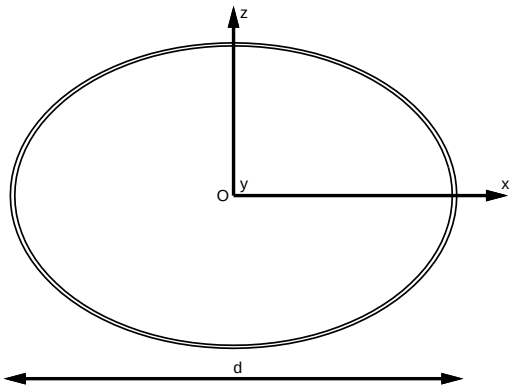

Fig. 4 Reference coordinate frame for the annular cross-section.

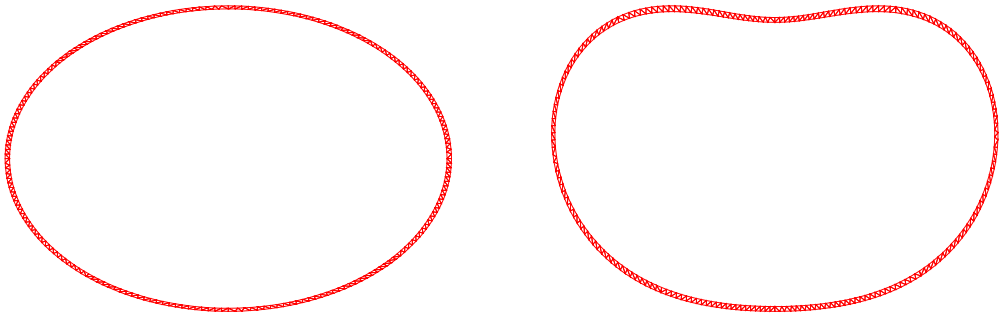

(a) $N = 1$ (b) $N = 4$

Fig. 5 Deformed loading point cross-sections in case of linear and fourth-order models, simply-supported beam.

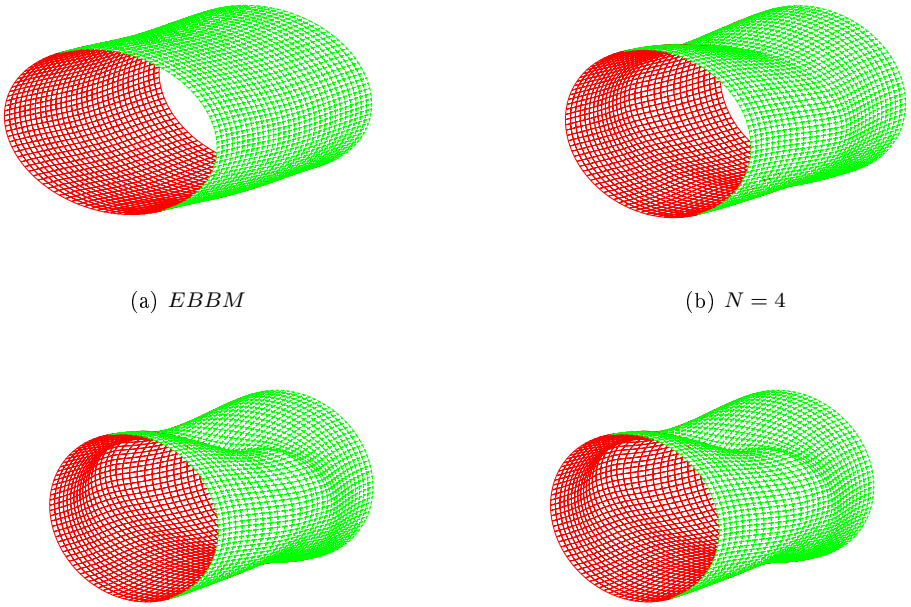

(a) $EBBM$ (b) $N = 4$

(c) $N = 8$ (d) $N = 11$

Fig. 6 Deformed beams in case of various theories, clamped-clamped beam.

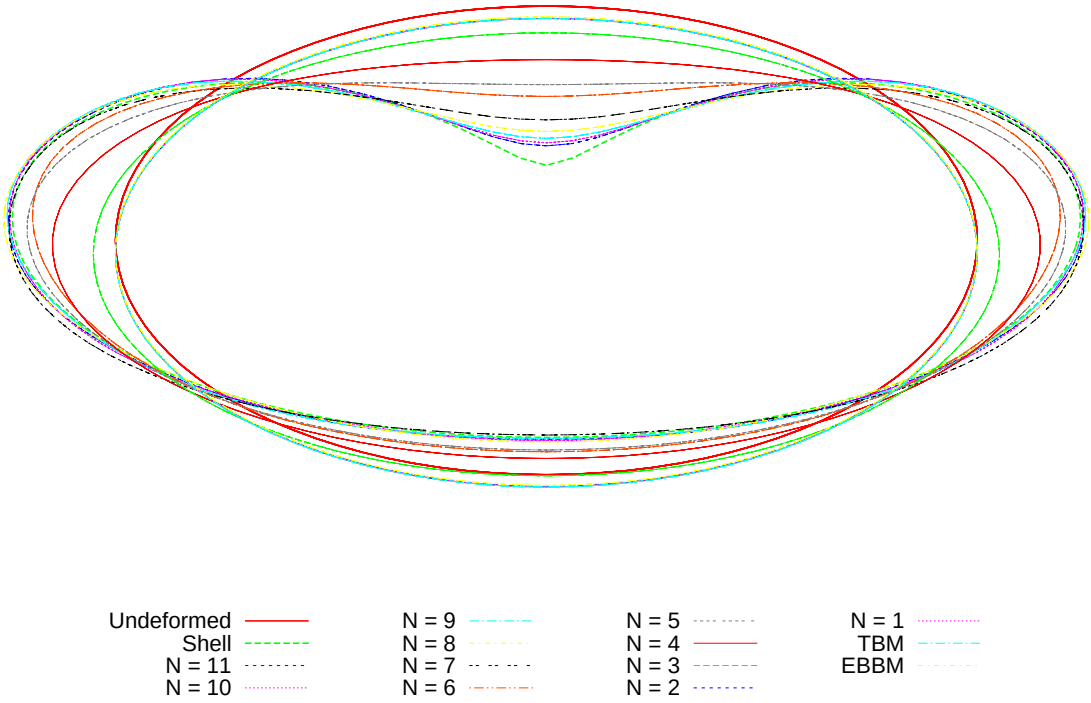

Fig. 7 Deformed configurations of the loading point cross-section for different beam theories and comparison with a shell model, clamped-clamped beam.

(a) Two lobes. (b) Three lobes.

Fig. 8 Two- and Three-lobe natural modes, clamped-clamped beam.

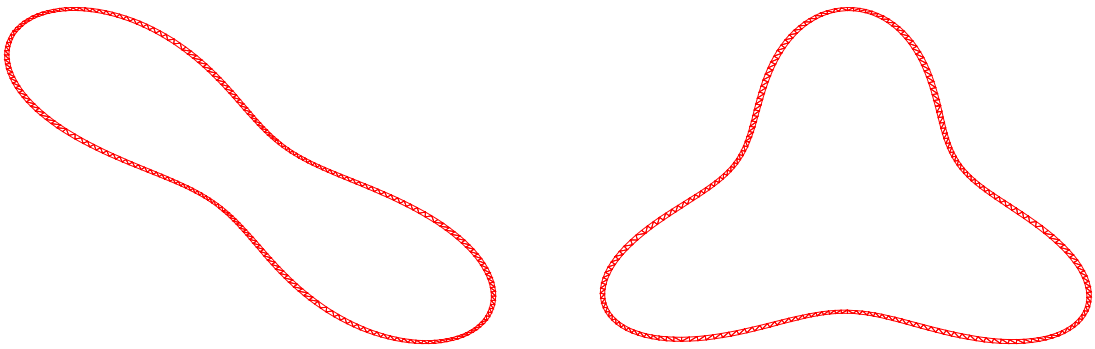

(a) Two lobes. (b) Three lobes.

Fig. 9 Two- and Three-lobe natural modes, 2-D sketches.